

Electronic Supplementary Information

**Facile Synthesis of Micro-Scale MOF Host-Guest with Long-Last
Phosphorescence and Enhanced Optoelectronic Performance**

Xiao-Gang Yang,^a Xiao-Min Lu,^a Zhi-Min Zhai,^{a,b} Ying Zhao,^{a,c} Xin-Yi Liu,^a Lu-Fang Ma^{*a,b} and Shuang-Quan Zang^{*b}

^aCollege of Chemistry and Chemical Engineering, Henan Province Function-Oriented Porous Materials Key Laboratory, Luoyang Normal University, Luoyang 471934, P. R. China.

^bCollege of Chemistry and Molecular Engineering, Zhengzhou University, Zhengzhou 450001, P. R. China.

^cState Key Laboratory of Coordination Chemistry, School of Chemistry and Chemical Engineering, Nanjing University, Nanjing 210093, P. R. China.

A. Experimental Section

1. Materials and general procedures.

Analytically pure $\text{Zn}(\text{NO}_3)_2 \cdot 6\text{H}_2\text{O}$, Na_2SO_4 , isophthalic acid (IPA), 2-methylimidazole (MIM), and Rhodamine B (RhB) were purchased from Energy Chemical. Co. Ltd. and used without further purification.

Powder X-ray diffraction analyses (PXRD) patterns were collected on a Bruker D8-ADVANCE X-ray diffractometer with Cu $K\alpha$ radiation ($\lambda = 1.5418 \text{ \AA}$). Measurements were made in a 2θ range of $5\text{--}50^\circ$ at room temperature with a step of 0.02° (2θ) and a counting time of 0.2 s/step. The operating power was 40 KV, 30 mA. The IR spectra were recorded in the range of $4000\text{--}400 \text{ cm}^{-1}$ on a Nicolet 6700 (Thermo) FT-IR spectrometer with KBr pellets. Thermogravimetric analysis (TGA) experiments were carried out using SII EXStar6000 TG/DTA6300 thermal analyzer from room temperature to 800°C under a nitrogen atmosphere at a heating rate of $10^\circ\text{C min}^{-1}$.

Single-crystal X-ray diffraction data for Y346 was collected at room temperature on an Oxford Diffraction SuperNova area-detector diffractometer using mirror optics monochromated Mo $K\alpha$ radiation ($\lambda = 0.71073 \text{ \AA}$). CrysAlisPro^[1] was used for the data collection, data reduction and empirical absorption correction. The crystal structure was solved by direct methods, using SHELXS-2014 and least-squares refined with SHELXL-2014^[2] using anisotropic thermal displacement parameters for all non-hydrogen atoms. The crystallographic data for Y346 are listed in Table S1 and Table S2. CCDC No. 1914021 contain the supplementary crystallographic data for Y346. This material can be obtained free of charge via <http://www.ccdc.cam.ac.uk/conts/retrieving.html>, or from the Cambridge Crystallographic Data Centre, 12 Union Road, Cambridge CB2 1EZ, UK; fax: (+44) 1223-336-033; or E-mail: deposit@ccdc.cam.ac.uk.

Photographs of MOF powder under UV excitation (365 nm) and day light were captured using a Canon digital camera (EOS 700D: the ISO value was 400, time of exposure was set to an automatic mode). Photoluminescence (PL) microscope images of RhB@Y346 microcrystals were taken under

LEICA DM5000 B fluorescence microscope. The morphology of all samples were investigated by using a field emission scanning electron microscope (SEM Sigma 500) equipped with an energy dispersive X-ray spectrum attachment (EDX Oxford Instruments Isis 300).

Room temperature PL spectra and time-resolved lifetime were conducted on an Edinburgh FLS1000 fluorescence spectrometer equipped with a xenon arc lamp (Xe900), nanosecond flash-lamp (nF900) and a microsecond flashlamp with time-resolved single photon counting–multi-channel scaling (MCS) mode. Upconversion fluorescence PL spectrum was excited by 980 nm laser on Edinburgh FLS1000 fluorescence spectrometer. UV-vis absorption spectra was measured using a Shimadzu UV-3600 plus UV-vis-NIR spectrophotometer.

Optoelectronic measurements were performed with a CHI 660E electrochemical analyzer (CH Instruments, Chenhua Co., Shanghai, China) in a standard three-electrode system using MOFs powder modified indium tin oxide (ITO) as the working electrode with a working area of 1.0 cm², a platinum wire electrode as a counter electrode, and Ag/AgCl as a reference electrode, 0.5 M sodium sulfate aqueous solution as electrolyte. The system was conducted in a quartz glass reactor ca. 50 cm³, and irradiated by a 300 W Xe lamp ($\lambda > 420$ nm for RhB@Y346). All the linear-sweep voltammograms (LSV) with a scan rate of 50 mV/s, electrochemical impedance spectroscopy (EIS) measurements recorded at the potential of -0.5 V potential in the frequency range of 100 kHz to 100 mHz and transient photocurrent responses with the on–off cycle's illumination at various bias potential (vs. Ag/AgCl) were tested in three-electrode system at ambient pressure and room temperature. Evolved H₂ were analyzed by an Agilent GC 7890A online gas chromatograph with thermal conductivity detector.

2. Synthesis of MOF samples.

2.1 Synthesis of Y346 bulk crystals.

A mixture of isophthalic acid (IPA, 1 mmol, 166 mg), 2-methylimidazole (MIM, 2 mmol, 164 mg), Zn(NO₃)₂ · 6H₂O (2 mmol, 595 mg) and H₂O (8 mL) was placed in a Teflon-lined stainless steel vessel,

heated to 180 °C for 12 h, and then cooled to room temperature naturally. Colorless block crystals of Y346 were obtained, which were washed with water and ethanol several times, then dried in natural environment.

2.2 Synthesis of Y346 microcrystals.

Addition of a solution of $\text{Zn}(\text{NO}_3)_2 \cdot 6\text{H}_2\text{O}$ (4 mmol, 1190 mg) in H_2O (2 mL) was added to a solution of 2-methylimidazole (4 mmol, 328mg) and iso-phthalic acid (2 mmol, 332 mg) in H_2O (8 mL) with vigorous stirring. Then, a large number of colorless microcrystal formed immediately, which were filtered, washed with water and ethanol several times, then dried in natural environment.

2.3 Synthesis of RhB@Y346 microcrystals .

2 mL $\text{Zn}(\text{NO}_3)_2 \cdot 6\text{H}_2\text{O}$ (4 mmol, 1190 mg) and RhB (0.3 or 3 mg for the low or high concentration encapsulation) aqueous solution was added into a mixture of 2-methylimidazole (4 mmol, 328mg), iso-phthalic acid (2 mmol, 332 mg) and in 8 mL H_2O with vigorous stirring, forming a large amount of bright violet precipitation immediately. Products were filtered, washed with water and ethanol several times, then dried in natural environment.

It should be noted that MIM is indispensable to the preparation of the Y346 host-guest microcrystals. MIM can not only be regarded as competitive ligand, but also serves as the base for the deprotonation of IPA ligands, accelerating the nucleation of crystallization.^[3] Thus, the guest RhB dye can be facilely in situ encapsulated druning the fast nucleation of Y346.

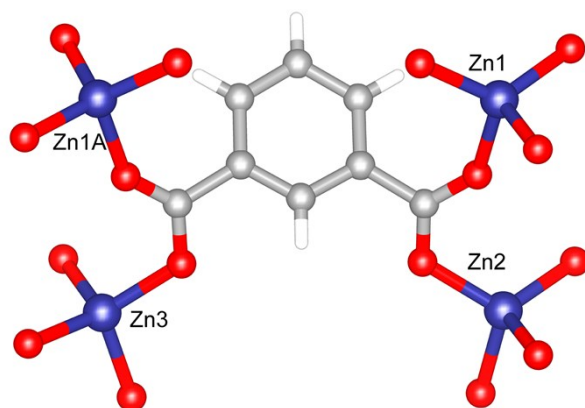
3. Preparation of working electrode

The ITO ($1 \times 4 \text{ cm}^2$) substrate is washed by ethanol, and water under ultrasonic processing for about 30 min then dried in natural environment. The MOF powders (10 mg) were added into 10 μL Nafion and 1 mL anhydrous ethanol mixed solution and ultrasonicated for 30 min to form suspension liquid. The working electrodes were prepared by dropping the above suspension (0.2 mL) onto the surface of the pre-treated ITO by controlling the coating area about 1 cm^2 , and allowing it to dry at room temperature.

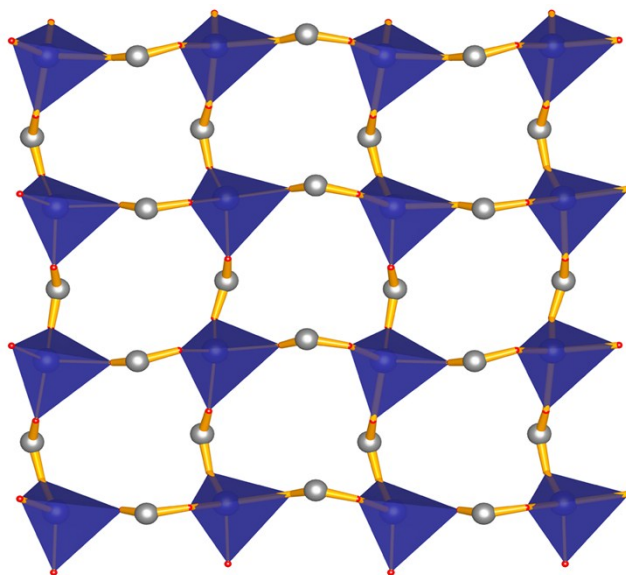
4. Electronic structure calculations of Y346

All calculations were performed with the periodic density functional theory (DFT) method using Dmol3^[4] module in Material Studio software package.^[5] The initial configuration was fully optimized by Perdew-Wang (PW91)^[6] generalized gradient approximation (GGA) method with the double numerical basis sets plus polarization function (DNP). The core electrons for metals were treated by effective core potentials (ECP). The self-consistent field (SCF) converged criterion was within 1.0×10^{-5} hartree atom⁻¹ and the converging criterion of the structure optimization was 1.0×10^{-3} hartree bohr⁻¹. The Brillouin zone is sampled by $1 \times 1 \times 1$ k-points, and test calculations reveal that the increase of k-points does not affect the results.

B. Supporting Figures



(a)



(b)

Figure S1. (a) Bridging mode of IPA ligand in Y346 (Symmetric code: $A = y+1/2, -x+2/3, z+1/4$), (b) Ball-and-stick/polyhedron view of the 2D -Zn-O-Zn- inorganic layer of Y346 along (001) plane.

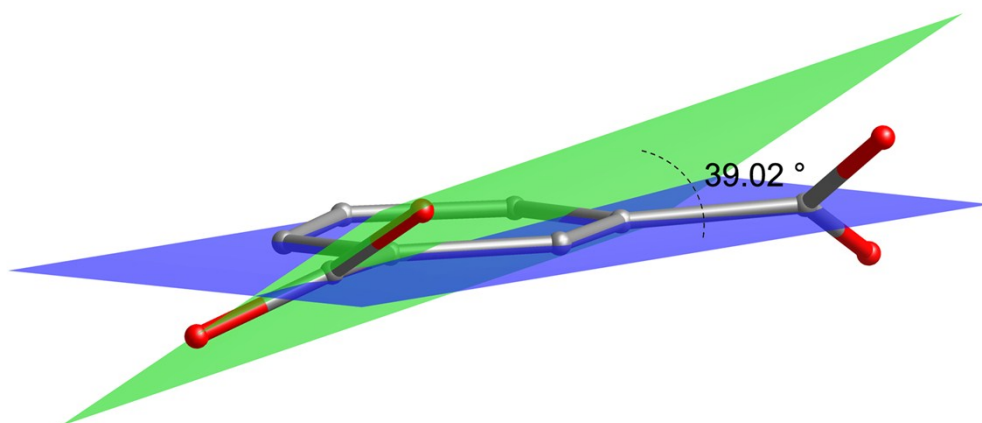


Figure S2. The torsion angle between benzene ring and carboxyl group of IPA in Y346.

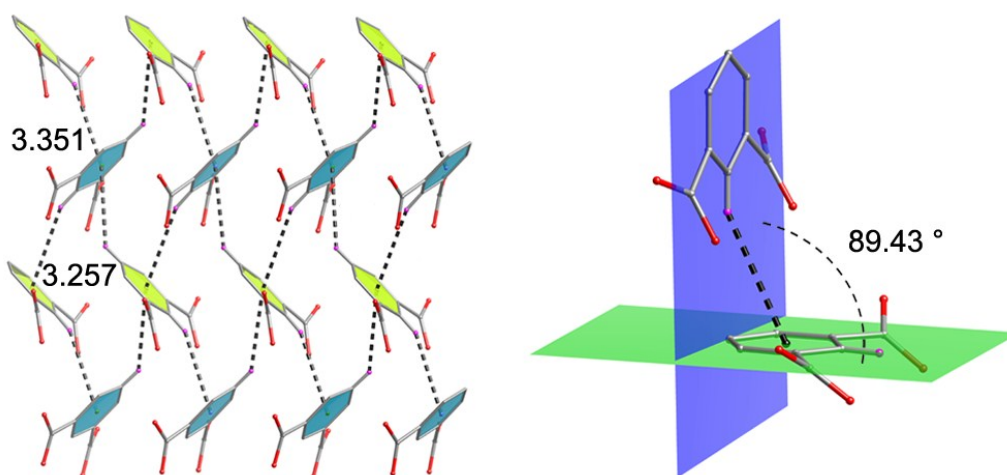


Figure S3. C-H... π supramolecular interactions between two approximately perpendicular benzene rings in Y346.

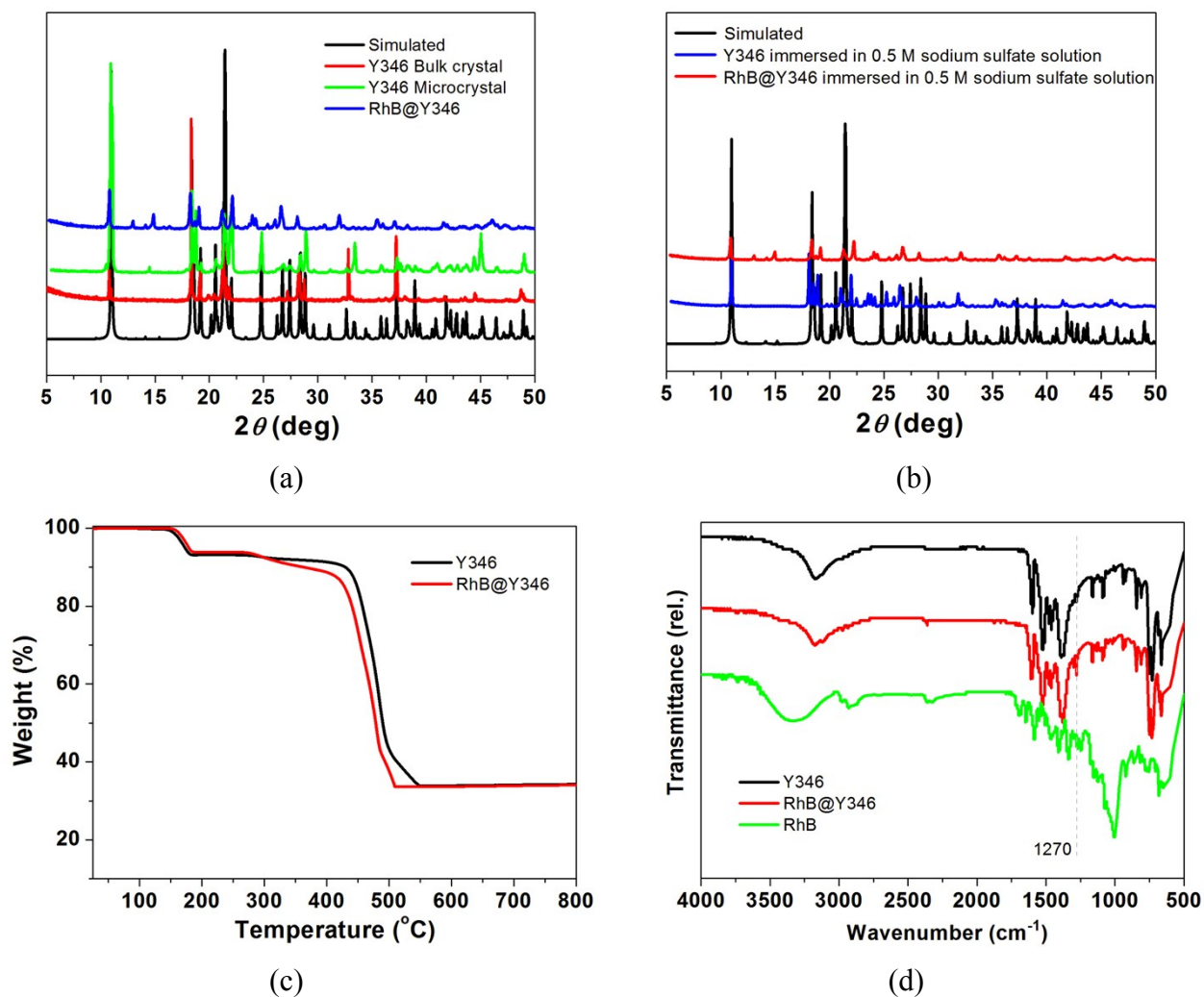


Figure S4. (a) PXRD patterns of Y346 bulk/microcrystal and RhB@Y346. (b) PXRD patterns of Y346 and RhB@Y346 powdered samples after immersed in 0.5 M Na_2SO_4 aqueous solution for 24 h. (c) TGA curves of Y346 and RhB@Y346 microcrystal. (d) FT-IR spectra of RhB, Y346 and RhB@Y346 microcrystal. The new band at $\sim 1270 \text{ cm}^{-1}$ can be assigned to the characteristic absorption peak of the aromatic oxide of RhB, indicating that the RhB dyes are encapsulated in the matrix of Y346.

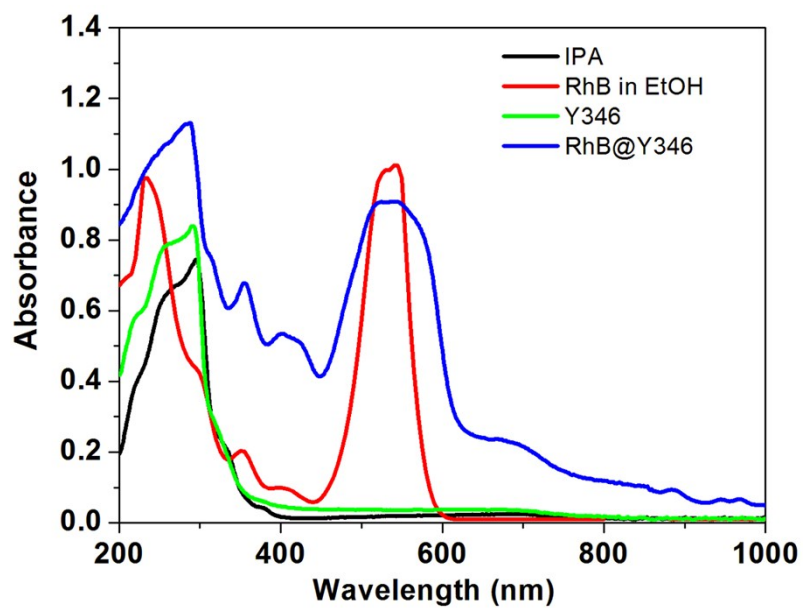
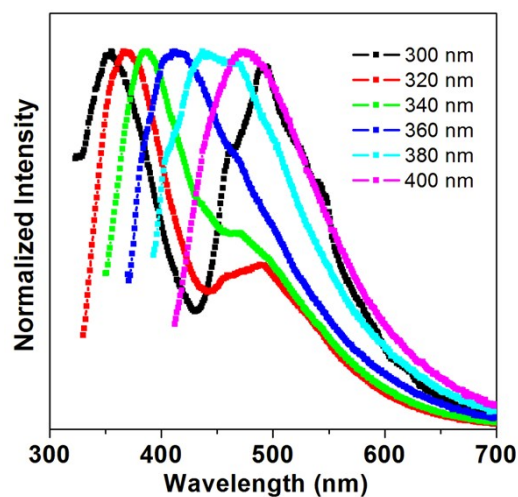
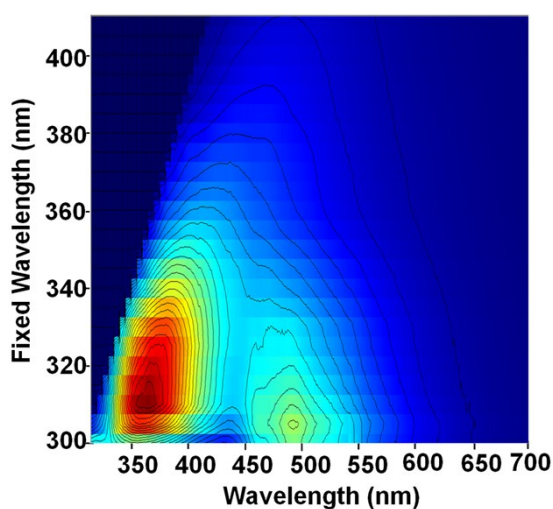


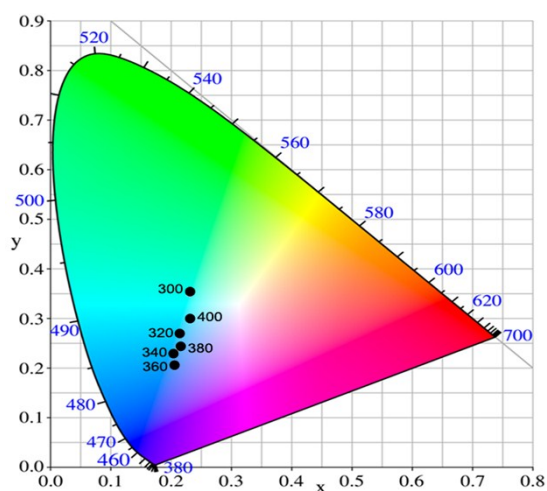
Figure S5. UV-vis-NIR absorption of IPA, RhB (ethanol solution), Y346 and RhB@Y346.



(a)

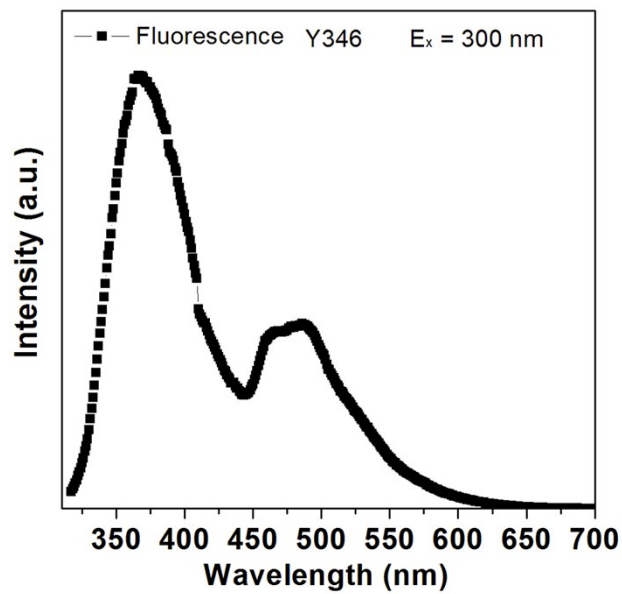


(b)

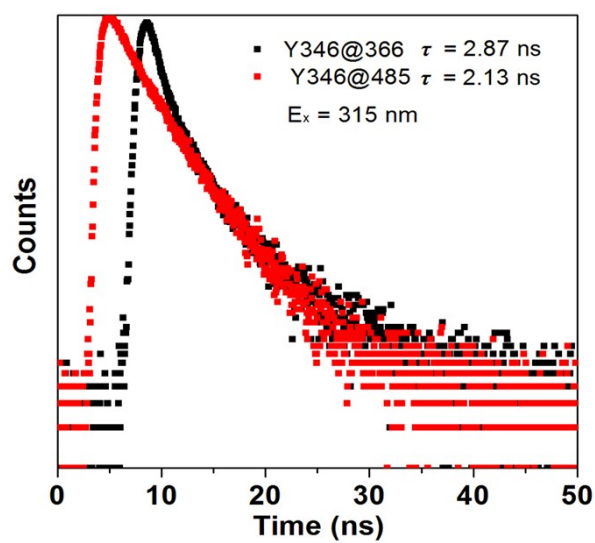


(c)

Figure S6. (a) Normalized excitation-dependent fluorescence spectra of Y346 with the excitation wavelength changed from 300 to 400 nm. (b) Excitation-dependent fluorescence mapping of Y346. (c) CIE-1931 chromaticity diagram showing the fluorescence emission of Y346 excited in the range of 300 to 400 nm.

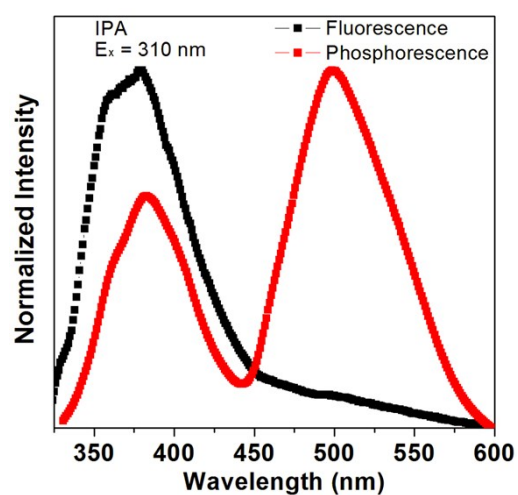


(a)

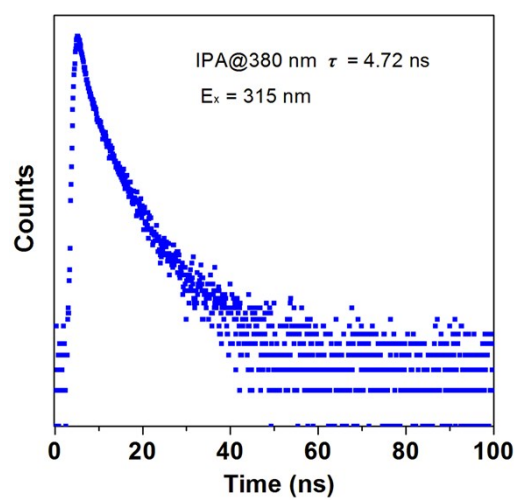


(b)

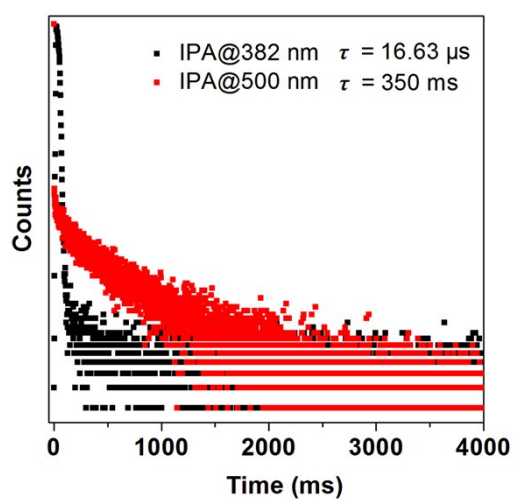
Figure S7. Fluorescence spectra (a) decay curves (b) of Y346.



(a)



(b)



(c)

Figure S8. Normalized fluorescence and phosphorescence spectra of IPA powder under 310 nm excitation. Fluorescence (b) and phosphorescence (c) decay curves of IPA powder.

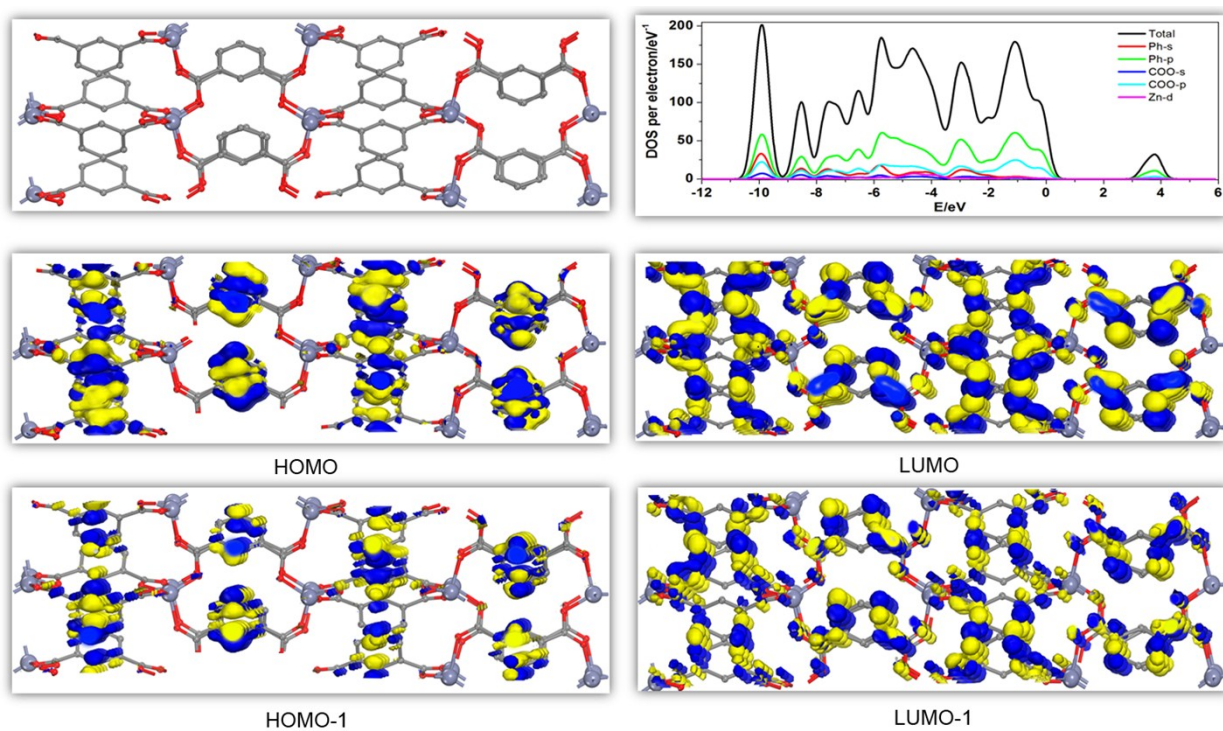
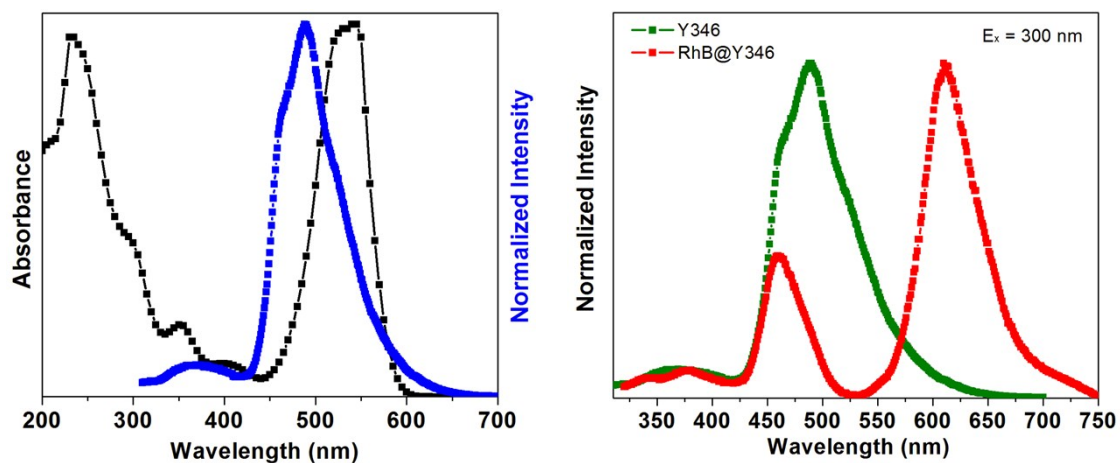
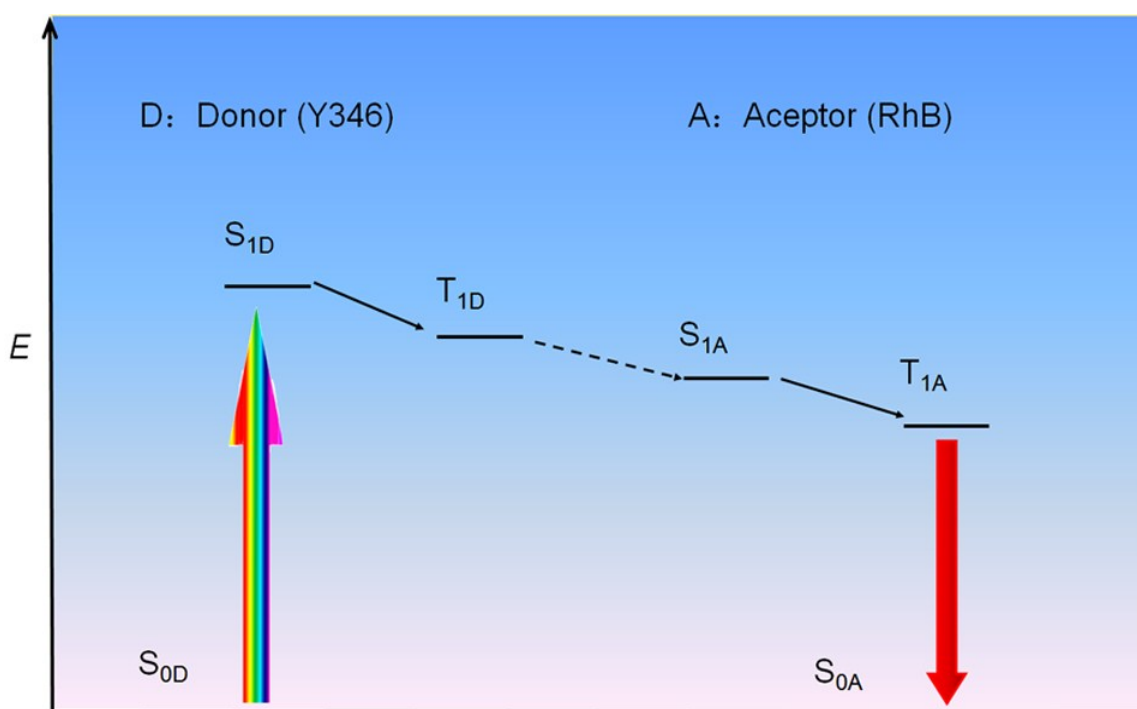


Figure S9. The 3D structure mode, TDOS and HOMO/LUMO orbital profiles based on PDFT calculations of Y346.



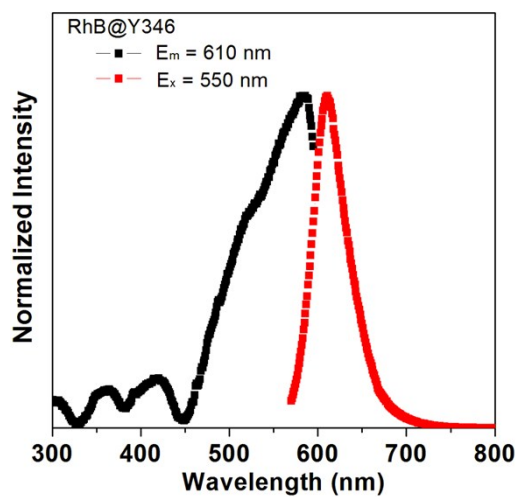
(a)

(b)

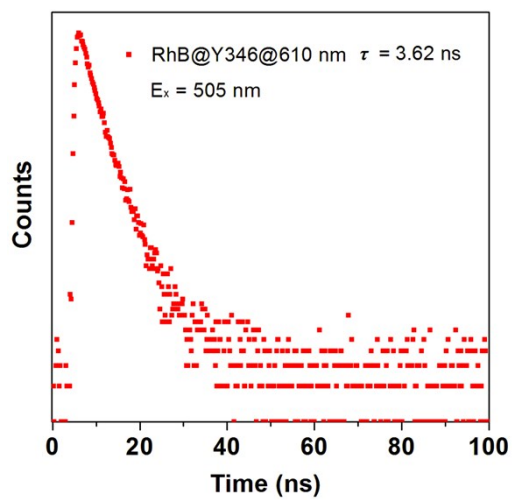


(c)

Figure S10. (a) Normalized UV-vis absorption of RhB (black, in ethanol) and phosphorescence emission spectrum (blue, excitation at 300 nm) of Y346. (b) Normalized phosphorescence spectra of Y346 and RhB@Y346. (c) A probable phosphorescence energy transfer (PET) process for RhB@Y346 host-guest system.

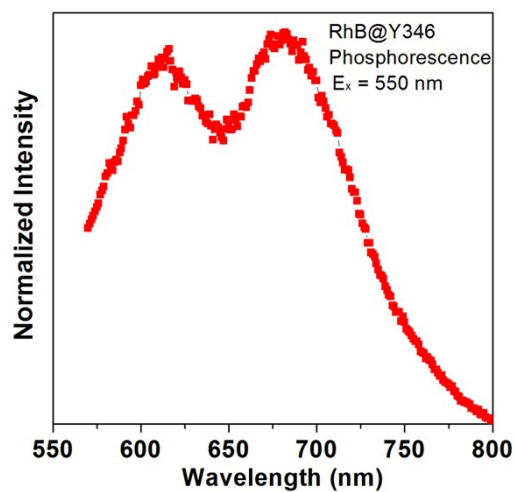


(a)

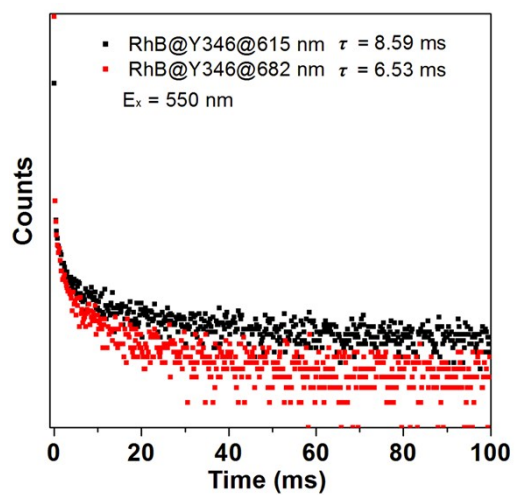


(b)

Figure S11. The excitation and fluorescence spectrum (a) as well as fluorescence decay curves (b) of RhB@Y346 under 505 nm excitation.



(a)



(b)

Figure S12. The phosphorescence spectrum (a) and decay curves (b) of RhB@Y346 under 550 nm excitation.

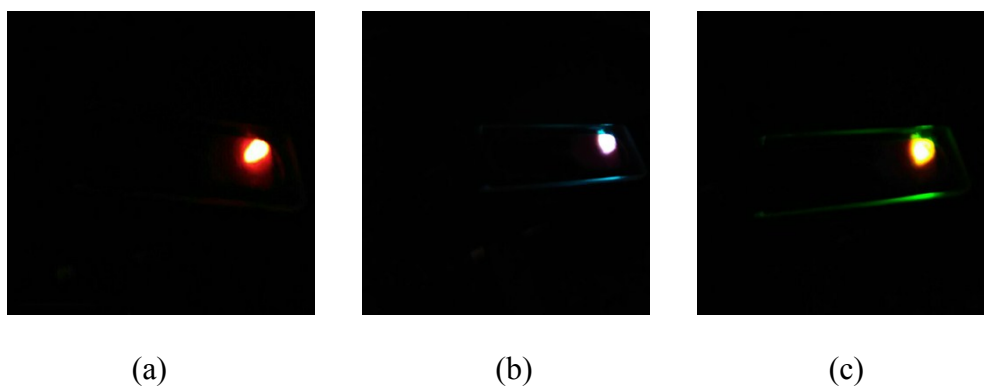


Figure S13. Photographs of RhB@Y346 under different wavelength pulsed light (100 Hz) excited by a microsecond flashing lamp at room temperature. (a): 360 nm, (b): 500 nm, (c): 550 nm.

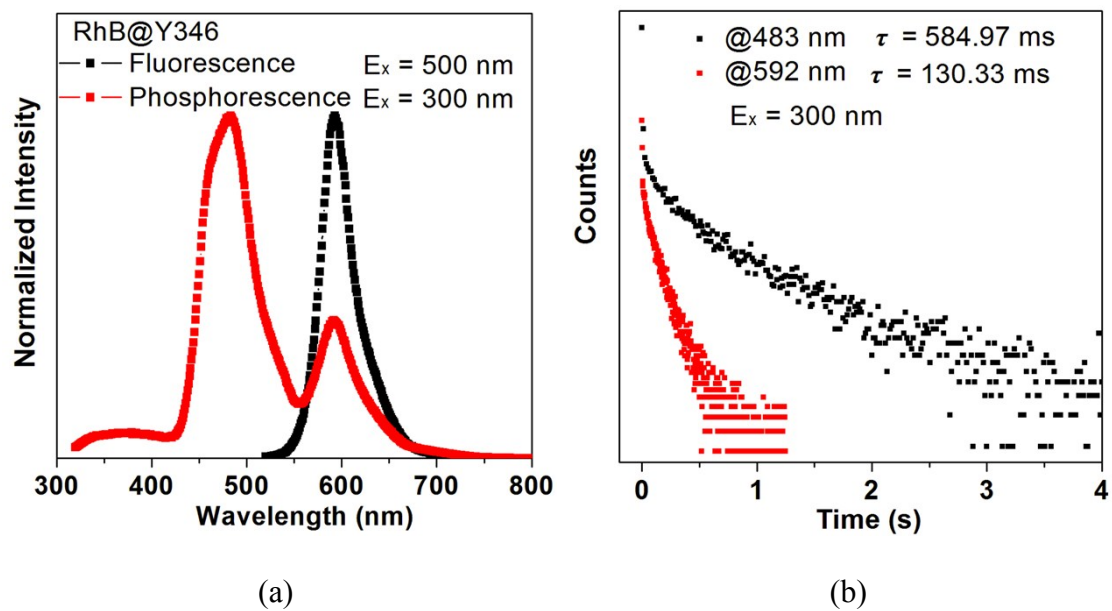


Figure. S14 (a) Normalized fluorescence and phosphorescence spectra of low concentrations RhB encapsulated in Y346 matrix. (b). Time-resolved phosphorescence decay curve of low concentration RhB encapsulated in Y346 matrix.

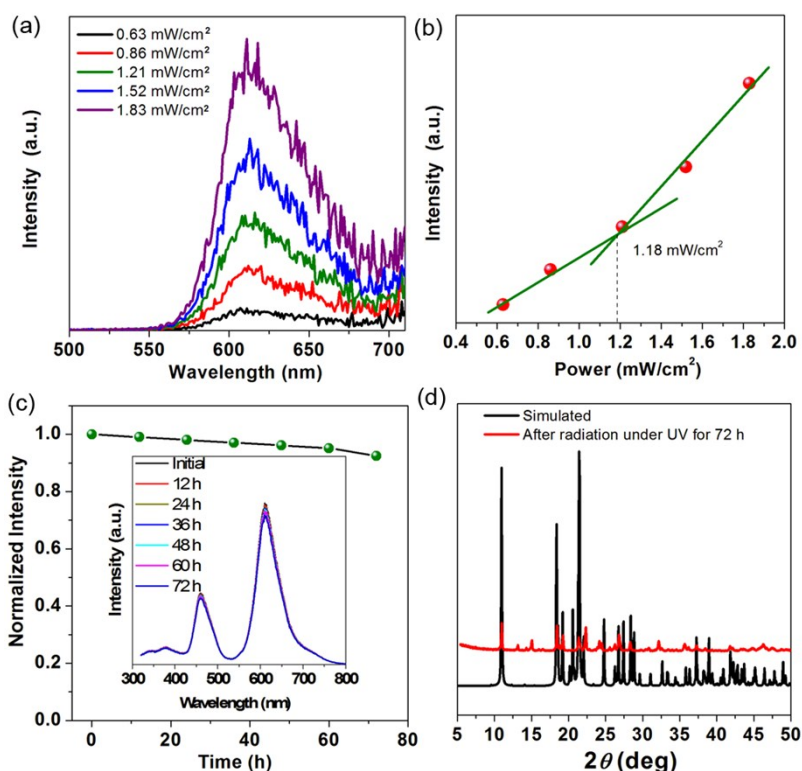


Figure S15. (a) Photoluminescence up-conversion spectrum of RhB@Y346 under excitation with 980 nm femtosecond pulse laser. (b) The changes in PL intensity with increasing pump density. (c) Photostability of RhB@Y346 under UV light radiation. Inset shows phosphorescence spectra of RhB@Y346 measured at different times. (d) PXRD patterns of RhB@Y346 powder after radiated under UV for 72 h.

The up-conversion emission further brought a new opportunity for the utilization of long-wavelength sunlight. Upon excitation with a femtosecond pulse 980 nm laser, red emission can also be detected (Fig. S15a). Radiated under high pump density, sharp peaks on the top of emission can be observed indicating the laser emission. The relation between PL intensity and pump density reveals the threshold of 1.18 mW cm⁻² (Fig. S15b). The rigid environment of Y346 can highly promote the photostability of the guest RhB dye. Radiated under continuous UV lamps (365 nm, 12 W), no obvious PL decrease was observed even after 72 h (Fig. S15c). PXRD patterns further demonstrate that the crystal structure of RhB@Y346 remains unchanged (Fig. S15d). Therefore, this work provide a new strategy to tune the phosphorescence performance of MOF materials with rare example of red emission and long term stability by in situ encapsulation.

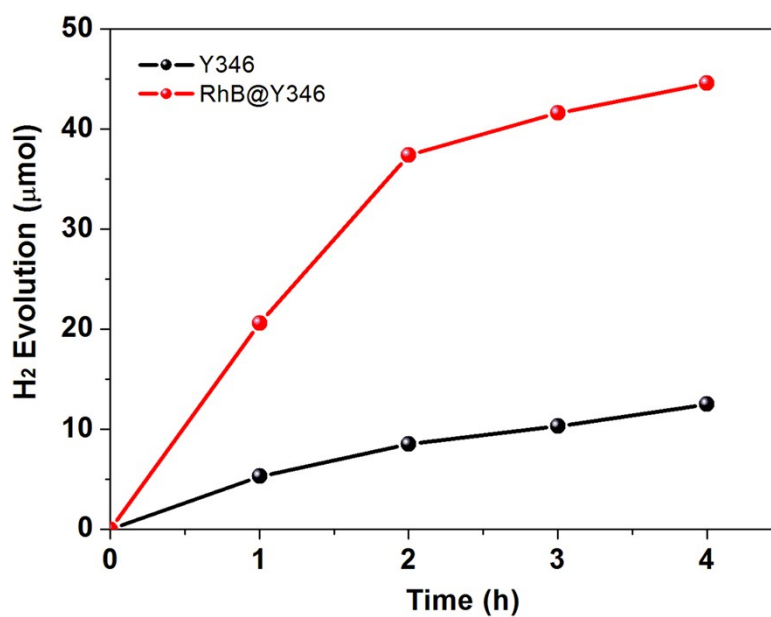


Figure. S16 Time courses of H₂ evolution with Y346 and RhB@Y346 photoanode at biases of -1 V vs. Ag/AgCl under 300 W Xe lamp light illumination.

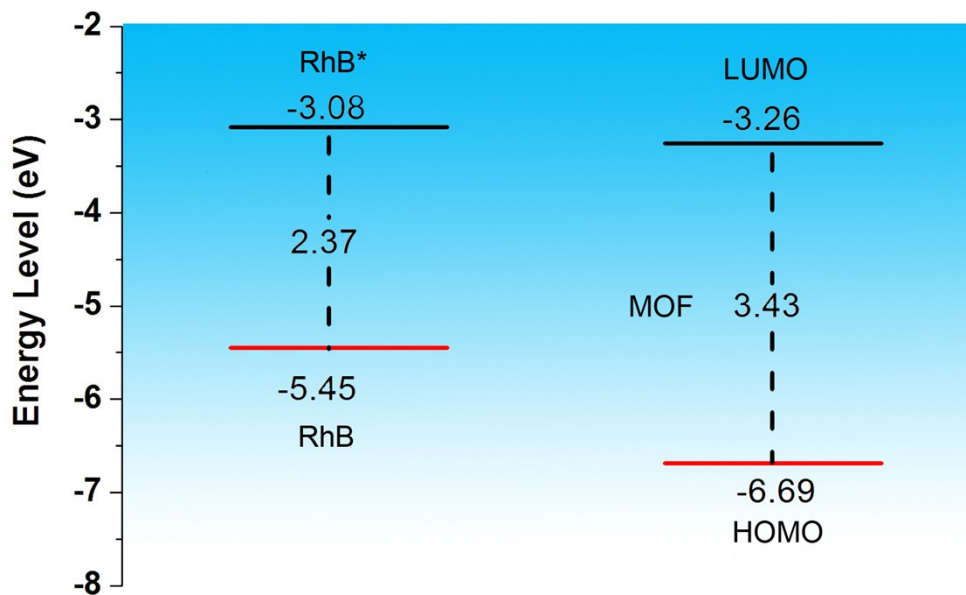
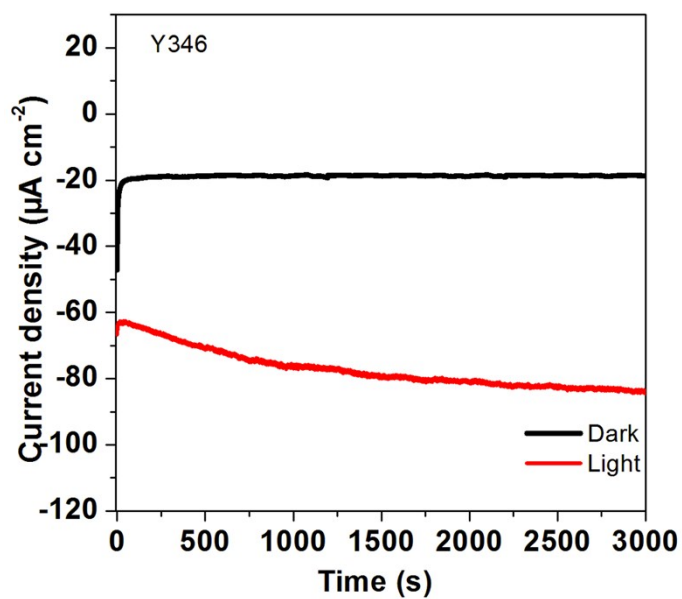
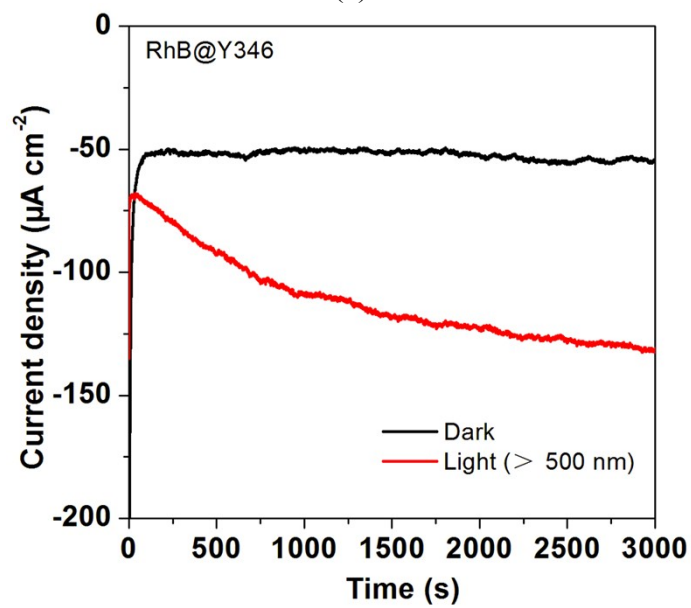


Figure. S17 The energy diagram of RhB and Y346.

Radiated under visible-light, the RhB dyes absorb visible-light to form electronically excited states RhB*. A comparison of energy level between RhB^[7] and Y346 indicates that the electron can directly transfer from the excited RhB* to the LUMO of Y346. The photocurrent on ITO anode modified by RhB@Y346 transfer to the Pt cathode instantaneously and subsequently reduces proton to H₂ under the addition of negative bias potential. In this way, the recombination of electrons and holes can be efficiently suppressed, thus, generating more free charges to improve efficiency of hydrogen evolution remarkably.



(a)



(b)

Figure S18. Constant potential electrolysis curves of Y346 (a) and RhB@Y346 (b) in 0.5 M Na_2SO_4 at bias potential of -0.5 V vs. Ag/AgCl under dark and light illumination.

C. Supporting Tables

Table S1. Crystallographic data for Y346.

Sample	[Zn(IPA)] (Y346)
Chemical formula	C ₈ H ₄ O ₄ Zn
Formula weight	229.48
CCDC NO.	1914021
Crystal system	tetragonal
Space group	<i>P</i> 4 ₃ 2 ₁ 2
<i>a</i> (Å)	9.63550(10)
<i>b</i> (Å)	9.63550(10)
<i>c</i> (Å)	32.1835(7)
<i>V</i> (Å ³)	2988.01(9)
<i>Z</i>	16
<i>D</i> (g cm ⁻³)	2.040
μ (mm ⁻¹)	3.258
<i>T</i> (K)	293.37(10)
Index ranges	-11 ≤ <i>h</i> ≤ 11, -11 ≤ <i>k</i> ≤ 11, -38 ≤ <i>l</i> ≤ 38
Data/restraints/parametes	2735/18/236
<i>R</i> _{int}	0.0605
Goof	1.164
<i>R</i> _{<i>I</i>} , <i>wR</i> ₂ [<i>I</i> > 2σ(<i>I</i>)]	0.0644, 0.1565
<i>R</i> _{<i>I</i>} , <i>wR</i> ₂ [all data]	0.0666, 0.1573

$$R_1 = \frac{\sum ||F_o| - |F_c||}{\sum |F_o|}, wR_2 = \left[\frac{\sum w(F_o^2 - F_c^2)^2}{\sum w(F_o^2)^2} \right]^{1/2}$$

Table S2. Selected bond distances /Å and bond angles /° for Y346.

[Zn(IPA)] (Y346)			
Zn1-O1	1.908(9)	Zn1-O3 ^{#1}	1.931(10)
Zn1-O5	1.984(11)	Zn1-O8 ^{#2}	1.993(11)
Zn2-O4 ^{#3}	1.989(11)	Zn2-O4 ^{#4}	1.989(11)
Zn2-O6 ^{#5}	1.922(10)	Zn2-O6	1.922(10)
Zn3-O2 ^{#4}	2.004(11)	Zn3-O2 ^{#6}	2.004(11)
Zn3-O7	1.912(10)	Zn3-O7 ^{#7}	1.912(10)
O1-Zn1-O3 ^{#1}	125.9(4)	O1-Zn1-O5	109.6(4)
O1-Zn1-O8 ^{#2}	106.4(4)	O3 ^{#1} -Zn1-O5	110.9(4)
O3 ^{#1} -Zn1-O8 ^{#2}	100.2(5)	O5-Zn1-O8 ^{#2}	100.0(5)
O4 ^{#3} -Zn2-O4 ^{#4}	96.7(7)	O6 ^{#5} -Zn2-O4 ^{#3}	112.7(4)
O6-Zn2-O4 ^{#4}	112.7(4)	O6 ^{#5} -Zn2-O4 ^{#4}	108.4(4)
O6-Zn2-O4 ^{#3}	108.4(4)	O6-Zn2-O6 ^{#5}	116.3(6)
O2 ^{#3} -Zn3-O2 ^{#6}	103.6(7)	O7 ^{#7} -Zn3-O2 ^{#3}	101.4(5)
O7 ^{#7} -Zn3-O2 ^{#6}	106.1(4)	O7-Zn3-O2 ^{#6}	101.4(5)
O7-Zn3-O2 ^{#3}	106.1(4)	O7-Zn3-O7 ^{#7}	134.9(7)

Symmetry operations: #1: 1/2+y, 3/2-x, 1/4+z; #2: 3/2-y, -1/2+x, -1/4+z; #3: 1/2+y, 1/2-x, 1/4+z; #4: 1/2+x, 1/2-y, 1/4-z; #5: 1-y, 1-x, 1/2-z; #6: 3/2-x, -1/2+y, 3/4-z; #7: 1+y, -1+x, 1-z; #8: 1/2-y, -1/2+x, -1/4+z.

D. Supporting References

- [1] CrysAlisPro, Rigaku Oxford Diffraction, Version 1.171.39.6a.
- [2] G. M. Sheldrick, *Acta Crystallogr. Sect. A.* 2008, **64**, 112.
- [3] C. Guo, Y. Zhang, Y. Guo, L. Zhang, Y. Zhang, J. Wang, *Chem. Commun.* 2018, **54**, 252.
- [4] (a) B. Delley, *J. Chem. Phys.* 1990, **92**, 508–517; (b) B. Delley, *J. Chem. Phys.* 2000, **113**, 756–7764.
- [5] Dmol³ Module, MS Modeling, Version 2.2; Accelrys Inc.: San, Diego, 2003.
- [6] J. P. Perdew, J. A. Chevary, S. H. Vosko, K. A. Jackson, M. R. Pederson, D. J. Singh, C. Fiolhais, *Phys. Rev. B.* 1992, **46**, 6671–6687.
- [7] Z. Xiong, L. L. Zhang, J. Ma and X. S. Zhao, *Chem. Commun.*, 2010, **46**, 6099–6101.